QUERIES - jop100520q

[AQ1] Please check author surnames for accuracy in typesetting.

[AQ2] This article and the abstract have been edited for clarity and flow throughout with the intent to retain original meaning. This includes text body and headings, all footnotes (affiliation and otherwise), any figures and their legends, and any tables and their legends, and any acronyms (where possible) that have been spelled out per journal style. Please read carefully for completeness and definition, and confirm or amend as needed.

[AQ3] Only those terms and phrases that match MeSH key words were retained. So that Key Words match MeSH terminology, "implant surface" and "in vivo" were removed. Please provide additional MeSH terms (total of 6 in all) as needed (consult http://www.nlm.nih.gov/mesh/MBrowser.html for common MeSH terms and phrases).

[AQ4] Please spell out LSD.

[AQ5] Please spell out V.

[AQ6] In reference 24, please provide location of publisher and name of editors of book

[AQ7] In reference 25, please provide location of publisher and page numbers.

Characterization of Five Different Implant Surfaces and Their Effect on Osseointegration: A Study in Dogs

[AQ1] Paulo G. Coelho,* Estevam A. Bonfante,† Roberto S. Pessoa,‡ Charles Marin,§ Rodrigo Granato,§ Gabriela Giro,‡ Lukasz Witek,* and Marcelo Suzuki‖

[AQ2] **Background:** Chemical modification of implant surface is typically associated with surface topographic alterations that may affect early osseointegration. This study investigated the effects of controlled surface alterations in early osseointegration in an animal model.

Methods: Five implant surfaces were evaluated: 1) alumina-blasted; 2) biologic blasting; 3) plasma; 4) microblasted-resorbable blasting media (microblasted RBM); and 5) alumina-blasted/acid-etched (AB/AE). Surface topography was characterized by scanning electron microscopy and optical interferometry, and chemical assessment by x-ray photoelectron spectroscopy. The implants were placed in the radius of six dogs, remaining 2 and 4 weeks in vivo. After euthanization, specimens were torqued-to-interface failure, and non-decalcified processed for histomorphologic, bone–implant contact, and bone area fraction occupied evaluation. Statistical evaluation was performed by one-way analysis of variance ($P<0.05$) and post hoc testing by the Tukey test.

Results: The alumina-blasted surface presented the highest average surface roughness and mean root square of the surface values, the biologic blasting the lowest, and AB/AE an intermediate value. The remaining surfaces presented intermediate values between the biologic blasting and AB/AE. The x-ray photoelectron spectroscopy spectra revealed calcium and phosphorus for the biologic blasting and microblasted RBM surfaces, and the highest oxygen levels for the plasma, microblasted RBM, and AB/AE surfaces. Significantly higher torque was observed at 2 weeks for the microblasted RBM surface ($P<0.04$), but no differences existed between surfaces at 4 weeks ($P>0.74$). No significant differences in bone–implant contact and bone area fraction occupied values were observed at 2 and 4 weeks.

Conclusion: The five surfaces were osseoconductive and resulted in high degrees of osseointegration and biomechanical fixation. *J Periodontol 2011;82:■■■-■■■.*

KEY WORDS

[AQ3] **Histology; osseointegration; torque.**

* Department of Biomaterials and Biomimetics, New York University, New York, NY.
† Department of Prosthodontics, University of São Paulo, Bauru School of Dentistry, Bauru, SP, Brazil.
‡ Department of Oral Diagnosis and Surgery, Universidade Estadual Paulista Júlio de Mesquita Filho, Faculdade de Odontologia de Araraquara, Araraquara, SP, Brazil.
§ Department of Dentistry, Universidade Federal de Santa Catarina, Florianópolis, SC, Brazil.
‖ Department of Prosthodontics, Tufts University School of Dental Medicine, Boston, MA.

Over the last four decades, clinical oral implantology has shown high survival rates over time (often exceeding 95% over 10 years[1,2]), and has been regarded as one of the most successful treatment modalities in dentistry. Such high success rates have been attributed to the excellent biocompatibility of titanium, which allows for intimate bone interaction at the optical microscopy resolution, regarded as osseointegration.[3-5]

Although high survival rates have been reported for endosseous devices, current research has emphasized implant design modification at various length scales (i.e., nanogeometry, microgeometry, and macrogeometry) to improve the early host–implant tissue response.[6] Such a potential decrease in healing time may result in reduction in treatment time frames through prosthetic restorations that could be placed in occlusal function at early implantation times.[6-8]

Among implant design modifications attempting to improve the host–implant response, implant surface modifications have been the most investigated.[3-8] The rationale for surface modification lays in the fact that it is the first part of the implant to interact with biofluids, potentially altering the cascade of events that leads to bone healing and intimate apposition with the device.[9]

Several reviews cover the large number of possibilities included in implant

doi: 10.1902/jop.2010.100520

surface modifications, and it is the general consensus that both rough surfaces (over smooth turned surfaces) and surface chemistry (additions of calcium-phosphorus–based bioceramics in various forms over non-coated surfaces) favor the early host–implant response.[4-6] From a historical perspective, dental implant surfaces evolved from the as-turned smooth surfaces toward textured rough surfaces, and recent research points toward chemical modification of moderately rough surfaces.[4-6,10,11]

From a temporal standpoint, both topographic and chemical surface modifications have drawn attention,[4-6,10,11] because both have shown promising results in in vitro[12] and in vivo models[13-20] relative to their moderately rough predecessors. Improvements have been achieved by alterations in surface wettability,[21] impregnation of calcium and phosphorus onto the titanium oxide layer,[18] deposition of discrete bioactive ceramics,[19,20,22] and through minor incorporation of other chemical elements, such as fluoride.[11,23] Because changes in surface chemistry typically result in surface texture during processing, controlling such variables to determine their relative effects in healing is a challenging task, and the largest direct comparison between various surfaces in a suitable in vivo model is desirable. Thus, the present study biomechanically and histomorphometrically evaluated the effect of various surface modifications in an animal model.

MATERIALS AND METHODS

The implants used in this study were screw-type implants with 3.75 mm of diameter and 8 mm in length provided by the manufacturer.¶ A total of 75 implants were used and divided into five groups according to surface treatment: 1) alumina-blasted; 2) biologic blasting; 3) plasma; 4) microblasted resorbable blasting media (microblasted RBM); and 5) alumina-blasted/acid-etched (AB/AE). Three implants from each group were used for surface characterization.

Surface Characterization

The surface characterization was accomplished with three different methods (n = 3 implants per surface). First, scanning electron microscopy# was performed at various magnifications under an acceleration voltage of 15 kV to observe surface topography in the different groups.

The second step was to determine the roughness parameters by optical interferometry** (IFM). Three implants of each surface were evaluated at the flat region of the implant cutting edges (three measurements per implant) and arithmetic mean of the absolute values of the surface height within the sampling area (Sa) and root mean square of the surface departures within the sampling area (Sq) parameters determined.[24,25] To separate roughness from waviness and shape for digital three-dimensional measurements, on a micrometer scale, a high-pass gaussian filter of 250 × 250 μm was used. After data normality verification, statistical analysis at 95% level of significance was performed by one-way analysis of variance.

The third procedure was the surface-specific chemical assessment performed by x-ray photoelectron spectroscopy (XPS). The implants were inserted in a vacuum transfer chamber and degassed to 10 to 7 torr. The samples were then transferred under vacuum to the XPS spectrometer.†† Survey spectra were obtained using a 165-mm mean radius concentric hemispherical analyzer operated at constant pass energy of 160 eV for survey and 80 eV for high-resolution scans. The take off angle was 90 degrees and a spot size of 150 × 150 μm was used. The implant surfaces were evaluated at various locations (three per implant).

Animal Model and Surgical Procedure

After approval of the Ethics Committee for Animal Research at the Federal University of Santa Catarina, Florianópolis, Brazil, six mongrel dogs were acquired and remained for 2 weeks in the animal facility before the first surgical procedure.

For surgery, three drugs were administered until general anesthesia achievement by intramuscular injection: 1) atropine sulfate (0.044 mg/kg); 2) xilazine chlorate (8 mg/kg); and 3) ketamine chlorate (15 mg/kg). The implantation site was the radius epiphysis, and the right limb of each animal provided implants that remained for 4 weeks in vivo, and the left limb provided implants that remained 2 weeks in vivo.

For implant placement, the surgical site was shaved with a razor blade and was followed by application of antiseptic iodine solution. An incision of ~5 cm through the skin and periosteum was performed and the periosteum was elevated for bone exposure.

Sequential drills were used following the manufacturer's recommendation under abundant saline irrigation at 1.200 rpm. The implants were placed in an interpolated distribution to minimize bias from different implantation sites (sites 1 to 5 from proximal to distal) along the radial epiphysis for torque and histomorphometric evaluation.

After placement the healing caps were inserted and sutured in layers with vicryl 4-0‡‡ for periosteum and nylon 4-0§§ for skin was performed. The animals

¶ Ti-6Al-4V, AB-Dental, Nir-galim, Israel.
# Philips XL 30, Eindhoven, The Netherlands.
** Phase View 2.5, Palaiseau, France.
†† Kratos Axis 165 multi-technique, Kratos Analytical, Chestnut Ridge, NY.
‡‡ Ethicon Johnson, Miami, FL.
§§ Ethicon Johnson.

stayed in the animal care facility and received antibiotics (benzyl penicillin benzatine, 20,000 IU/kg) and anti-inflammatory (ketoprofen 1% 1 ml/5 kg) medications to control pain and infection. Euthanasia was performed after 4 weeks by anesthesia overdose and the limbs were retrieved by sharp dissection.

For torque testing, the radius was adapted to an electronic torque machine equipped with a 500-Ncm torque load cell.‖‖ Custom machined tooling was adapted to each implant's internal connection and the bone block was carefully positioned to avoid specimen misalignment during testing. The implants were torqued in a counterclockwise direction at a rate of ~0.196 radians per minute until a 10% decrease in maximum value was recorded, and a torque versus displacement curve was recorded for each specimen. The rationale for this procedure was to minimize interface damage before histologic procedures.[13,14]

The implants in bone were then referred to histomorphometric analysis. The implants in bone were reduced to blocks and then immersed in 10% buffered formalin solution for 24 hours. The blocks were then washed in running water for 24 hours, and gradually dehydrated in a series of alcohol solutions ranging from 70% to 100% ethanol. After dehydration, the samples were embedded in a methacrylate-based resin¶¶ according to the manufacturer's instructions. The blocks were then cut into slices (~300 μm thickness) aiming the center of the implant along its long axis with a precision diamond saw,## glued to acrylic plates with an acrylate-based cement, and a 24-hour setting time was allowed before grinding and polishing. The sections were reduced to a final thickness of ~30 μm by means of a series of abrasive papers*** (400, 600, 800, 1,200, and 2,400) in a grinding/polishing machine††† under water irrigation.[26] The sections were then stained with toluidine blue and referred to optical microscopy for histomorphologic evaluation.

The bone–implant contact (BIC) was determined at ×50 to ×200 magnification‡‡‡ by means of computer software.§§§ The regions of BIC along the implant perimeter were subtracted from the total implant perimeter, and calculations were performed to determine the BIC. The bone area fraction occupied (BAFO) between threads in trabecular bone regions was determined at ×100 magnification by means of computer software. The areas occupied by bone were subtracted from the total area between threads, and calculations were performed to determine the BAFO (reported in percentage values of bone area fraction occupied).[27]

Preliminary statistical analyses showed no effect of implant site (i.e., there were no consistent effects of positions 1 to 5 along the radius) on all measurements. Therefore, site was not considered further in the analysis. Statistical evaluation of torque to interface fracture, BIC, and BAFO was performed by one-way analysis of variance. Statistical significance was indicated by P levels <5%, and post hoc testing used the Fisher LSD test. [AQ4]

RESULTS

Electron micrographs of all implant surfaces are presented in Figures 1 and 2 and their representative 250 × 250 μm IFM three-dimensional reconstructions are shown in Figure 3. Their respective Sa and Sq values are presented in Figure 4A. The surface texture observed at intermediate and high magnification levels (Figs. 1 and 2) and the IFM reconstruction (Fig. 3) revealed morphologic differences among groups. Although similar morphology was observed for the alumina-blasted, microblasted RBM, and AB/AE surfaces, scanning electron micrographs showed that the biologic-blasting presented rough regions from the grit-blasting procedure along with flat regions with the original as-machined grooves. The plasma group surface morphology presented a rough surface with rounded morphology compared to the other groups (Figs. 1E and 1F). Residual blasting media particles were only observed on the alumina-blasting (Figs. 1A and 1B) and biologic-blasting surfaces (Figs. 1C and 1D).

The IFM measurements presented significant differences for both Sa and Sq values (Figs. 4A and 4B), where the alumina-blasted surface presented the highest, the biologic-blasting the lowest, and AB/AE the intermediate value. The other surfaces presented intermediate values between the biologic-blasting and AB/AE (non-significant between groups) (Figs. 4A and 4B).

The XPS spectra evaluated the presence of aluminum, phosphorus, calcium, nitrogen, titanium, carbon, V, oxygen, and sodium for the different surfaces (Figs. 4A and 4C). The highest aluminum concentration was [AQ5] observed for the alumina-blasting surface. The highest calcium and phosphorus concentration was observed for the biologic-blasting surface, followed by the microblasted RBM at much lower concentrations and all other surfaces without the presence of these chemical elements. No titanium was detected for the plasma-treated surface, and the second lowest titanium value was observed for the biologic-blasting surface. The highest carbon values were observed for the plasma and alumina-blasting surfaces, and the highest oxygen levels were observed for the plasma,

‖‖ Test Resources, Minneapolis, MN.
¶¶ Technovit 9100, Heraeus Kulzer, Wehrheim, Germany.
Isomet 2000, Buehler, Lake Bluff, IL.
*** SiC abrasive papers, Buehler.
††† Metaserv 3000, Buehler.
‡‡‡ Leica DM2500M, Leica Microsystems, Wetzlar, Germany.
§§§ Leica Application Suite, Leica Microsystems.

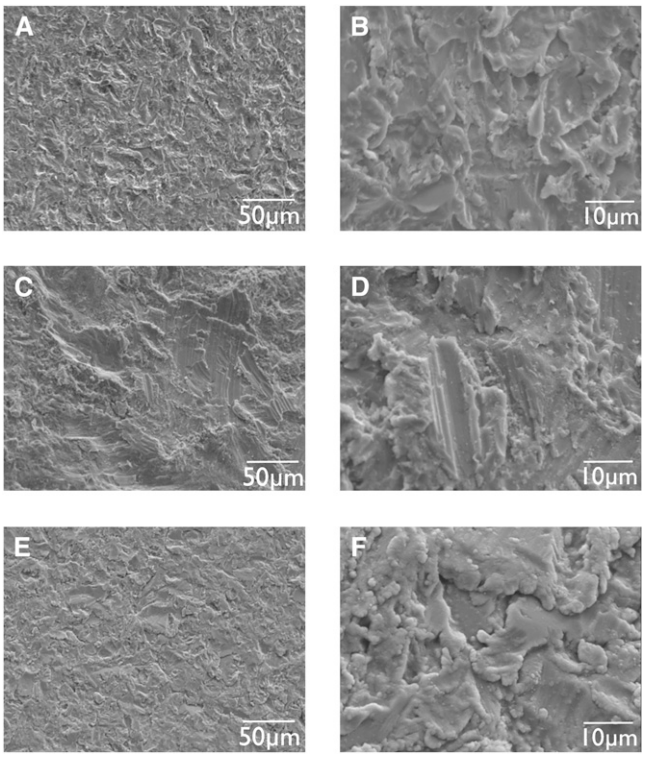

Figure 1.
*Scanning electron micrographs of the alumina-blasting **(A** and **B)**, biologic-blasting **(C** and **D)**, and plasma **(E** and **F)** surfaces.*

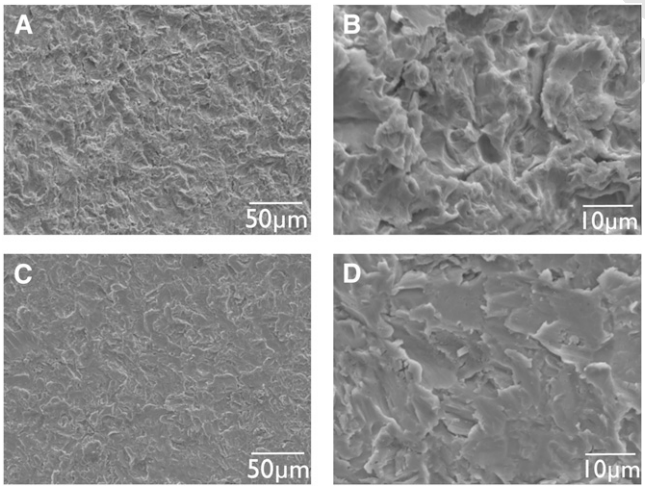

Figure 2.
*Scanning electron micrographs of the microblasted RBM **(A** and **B)** and AB/AE **(C** and **D)** surfaces.*

microblasted RBM, and AB/AE surfaces (Figs. 4A and 4C).

The animal surgical procedures and follow-up demonstrated no complications regarding procedural conditions, postoperative infection, or other clinical concerns. No implants were excluded from the study because of clinical instability immediately after euthanization.

The biomechanical testing results showed that significantly higher torque to interface fracture occurred for the microblasted RBM surface relative to others at 2 weeks ($P<0.04$), but that at 4 weeks no differences were observed between surfaces ($P>0.74$) (Figs. 5A and 5B).

The non-decalcified sample processing after controlled torque testing showed intimate bone contact with all implant surfaces at regions of cortical and trabecular bone. Higher magnification of the bone–implant interface region showed that the non-decalcified sections obtained after biomechanical testing presented minimal morphologic distortion because of mechanical testing bone disruption (Fig. 6).

Qualitative evaluation of the toluidine blue–stained thin sections revealed no morphologic differences between surfaces at 2 weeks (Figs. 6A through 6C) and 4 weeks (Figs. 6D through 6F) in vivo, where intimate contact between cortical (Figs. 6A, 6B, 6D, and 6E) and trabecular (Figs. 6C and 6F) bone was observed. In addition, different healing patterns were observed at different regions along the implant bulk, depending on the interplay between implant geometry and surgical instrumentation dimensions.

At the region of the implant where the inner thread diameter was larger or equal the final surgical drilling dimension allowing intimate contact between implant surface and cortical bone occurred immediately after implantation, substantial bone remodeling in proximity with the implant surface occurred between 2 (Fig. 6A) and 4 (Fig. 6D) weeks in vivo for all groups. Although at 2 weeks in vivo old bone remodeling was observed along with regions of newly formed woven bone (Fig. 6A), at 4 weeks substantial woven bone was observed in proximity with the implant surface (Fig. 6D).

At regions where a healing chamber was formed because of the formation of a space between the outer diameter of the surgical instrumentation and the inner diameter of the implant thread, woven bone formation was observed throughout the space of the chamber and directly onto the implant surface at 2 weeks in vivo (Fig. 6B). At 4 weeks, initial woven bone replacement by lamellar bone was observed throughout the healing chamber (Fig. 6E).

At trabecular bone regions, newly formed woven bone was observed at 2 weeks (Fig. 6C), and initial woven bone replacement by lamellar bone was observed at 4 weeks (Fig. 6F) at regions in proximity with all implant surfaces.

The histomorphometric results demonstrated no significant differences between surfaces for both BIC and BAFO at 2 and 4 weeks in vivo (BIC $P>0.26$ and $P>0.09$, respectively; BAFO $P>0.94$ and $P>0.09$, respectively; Figs. 5C through 5F).

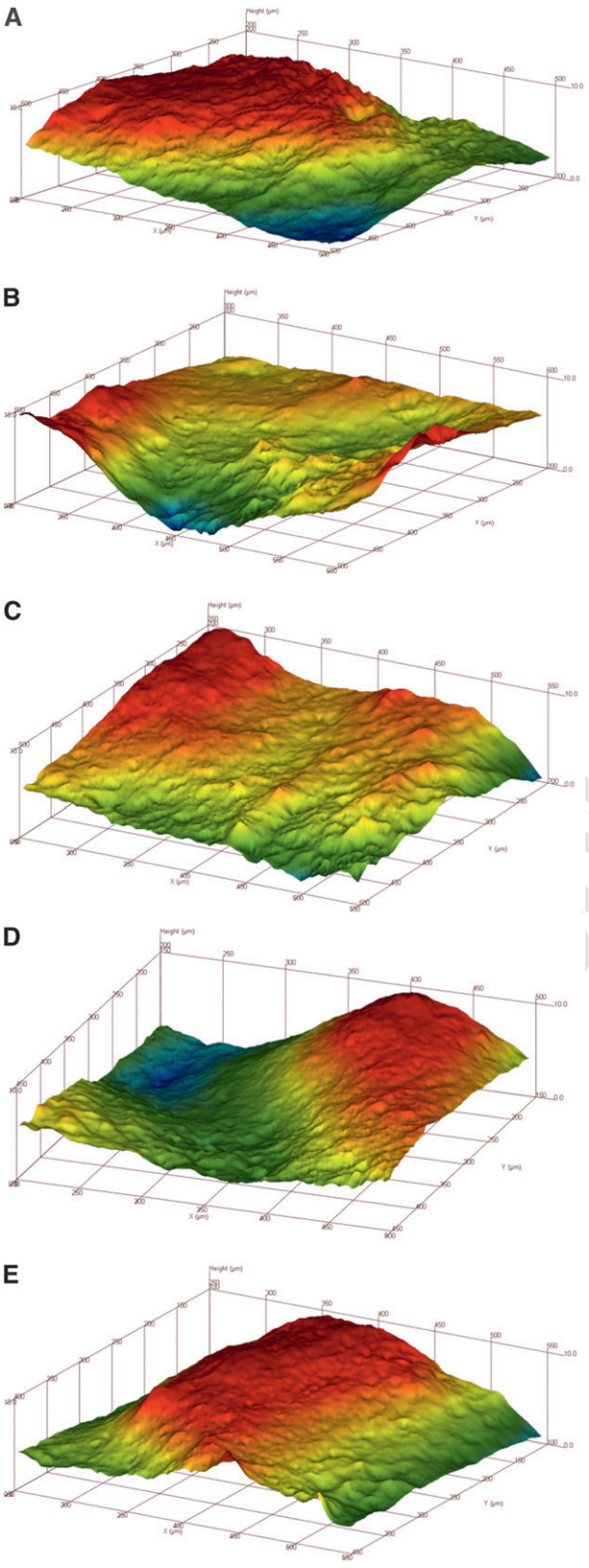

Figure 3.
*IFM three-dimensional reconstructions of the alumina-blasting **(A)**, biologic-blasting **(B)**, plasma **(C)**, microblasted RBM **(D)**, and AB/AE **(E)** surfaces.*

A	XPS Spectra									IFM	
	Al2p	P2p	Ca2p	N1s	Ti2p	C1s	V2p3	O1s	Na1s	Sa (µm)	Sq (µm)
Alumina Blasted	5.89	-	-	1.12	4.72	52.72	0.12	32.95	0.52	2.66 (0.42)	3.41 (0.38)
Biological Blasting	0.55	8.55	12.7	0.37	1.33	38.57	0.06	37.64	0.09	0.92 (0.38)	1.17 (0.47)
Plasma	1.49	-	-	0.31	-	48.96	0.03	48.05	0.53	1.13 (0.40)	1.50 (0.51)
Microblasted RMB	2.96	2.57	0.67	0.89	7.17	36.59	0.34	47.03	1.43	1.53 (0.51)	1.80 (0.60)
AB/AE	1.54	-	-	0.87	8.31	37.48	0.25	49.53	1.03	1.88 (0.49)	2.29 (0.60)

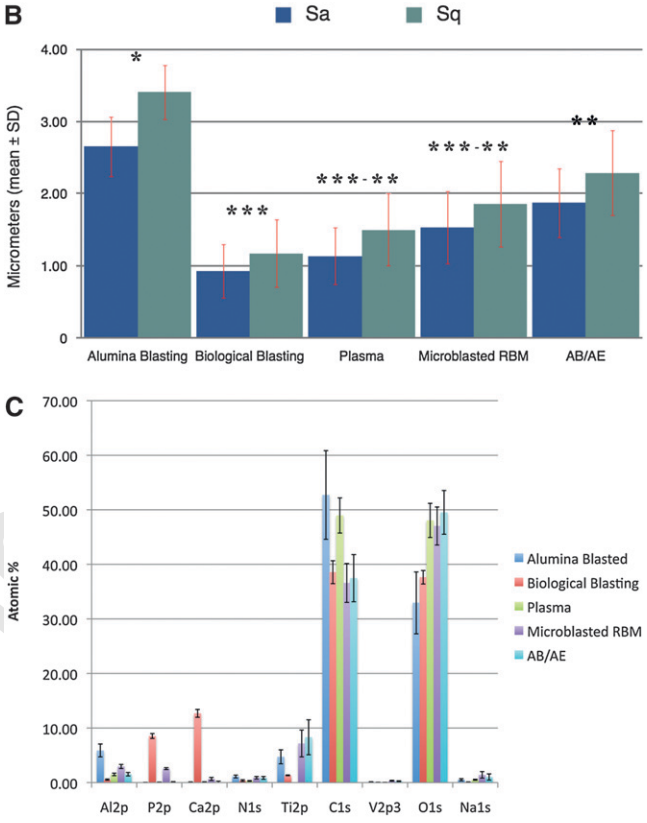

Figure 4.
***(A)** Average chemical composition for the different surfaces as observed in the XPS spectra and the statistics summary for the Sa and Sq values (mean ± SD). **(B)** Roughness parameters Sa and Sq (mean ± SD) for the different surfaces. The number of asterisks denotes statistically homogeneous groups. **(C)** Surface atomic compositions for the different implant surfaces (mean ± SD).*

DISCUSSION

Implant surfaces have evolved from the smooth as-machined (as-turned) surfaces toward the now considered standard rough surfaces fabricated by a variety of methods, which include all those used to fabricate the different surfaces evaluated in the present study.[6] Compared to published data, the obtained surface roughness values in the present study were higher because of the larger filter size used during IFM measurements (the smaller the filter, the lower the Sa and Sq values obtained[28]). Nonetheless, the relative differences among groups are in agreement with previously published work.[4,5] Although

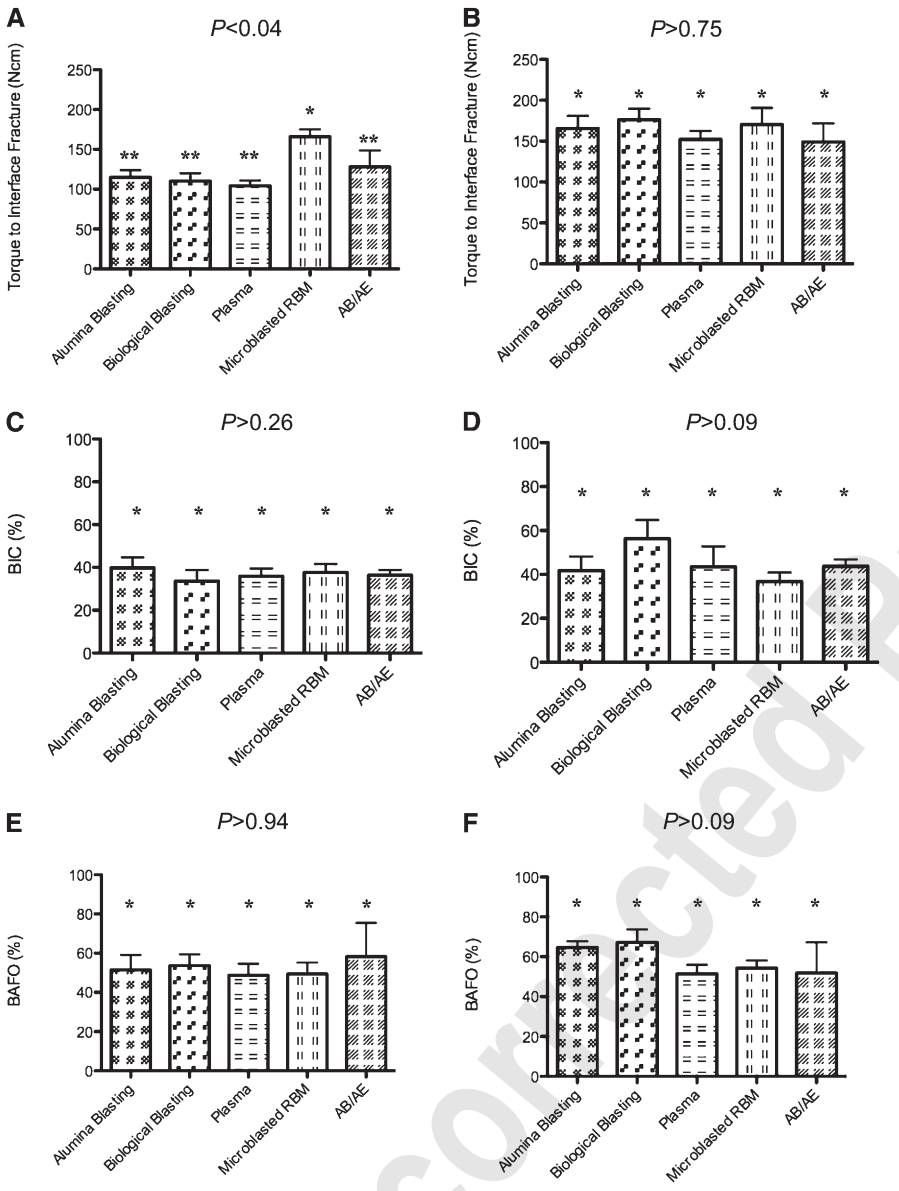

Figure 5.
*Torque–interface fracture statistics summary (mean ± 95% confidence interval [CI]) for the different surfaces at **(A)** 2 weeks and **(B)** 4 weeks in vivo. BIC statistics summary (mean ± 95% CI) for the different surfaces at **(C)** 2 weeks and **(D)** 4 weeks in vivo. BAFO statistics summary (mean ± 95% CI) for the different surfaces at **(E)** 2 weeks and **(F)** 4 weeks in vivo. The number of asterisks denotes statistically homogeneous groups.*

the alumina-blasting group presented a textured surface along with blasting media particles embedded on the surface, the AB/AE surface presented a reduced surface roughness without evidence of particle embedding in the surface, demonstrating the effectiveness of acid-etching on further cleaning the surface after blasting procedures.

Specific to the incorporation of calcium- and phosphorus-based bioactive ceramics, although both the biologic-blasting and microblasted RBM surfaces were blasted with resorbable blasting media, the blasting machinery and subsequent surface cleaning differences resulted in different textures and chemistries. First, because of the lower hardness of RBM compared to alumina, lower degrees of roughness were observed compared to both alumina-blasting and AB/AE samples. Second, observation of the electron micrographs for the biologic-blasting and microsblasted RBM revealed more consistent spatial distribution of texture for the microblasted RBM surface, which unlike the biologic-blasting group did not show regions where machining grooves were apparent between textured regions. Third, different post-blasting procedures resulted in calcium–phosphorus particles throughout the biologic blasting surface and high degrees of calcium and phosphorus on its surface chemistry spectrum, and chemical impregnation[10] of calcium and phosphorus elements on the microblasted RBM surface.

Although no detail was provided regarding the plasma source composition and temperature for the plasma group, it is apparent from the electron micrographs that the surface was previously blasted and that the texture was affected by the plasma processing. Such statements can be rationalized because rounded structures were observed in the plasma group compared to sharp defined peaks and valleys observed in all other groups. In addition, a substantial chemical shift was achieved by such a method, where titanium was not detected along with increased carbon and oxygen in the surface composition. This chemical shift may have originated from a substantial increase in the surface oxide layer, or possibly by a high surface energy characteristic that may have readily adsorbed carbon-based species from the atmosphere during sample preparation.

The torque–interface fracture results showed high biomechanical fixation values for all implant surfaces at 2 weeks (significantly higher for the microblasted RBM compared to other surfaces), and a

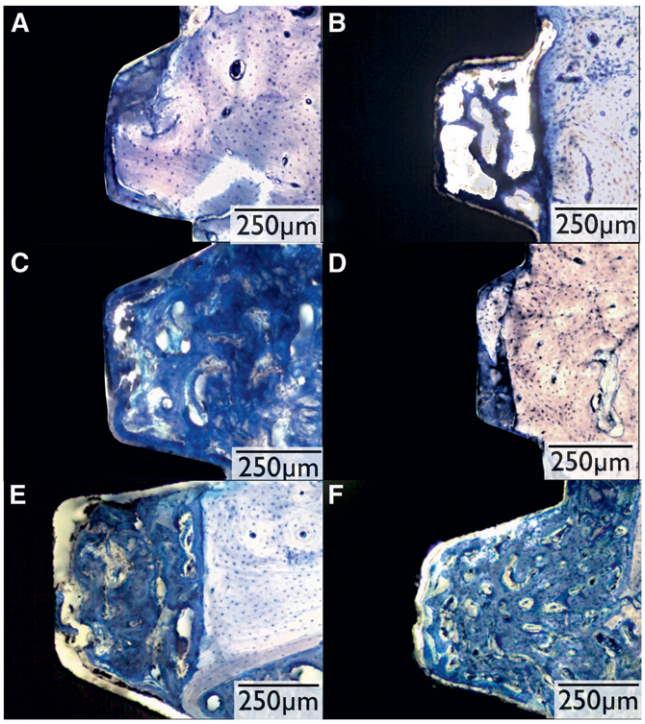

Figure 6.
*Representative histologic section for all groups at 2 and 4 weeks in vivo: **(A** and **D**, respectively**)** at a region where intimate contact between implant surface and cortical bone occurred immediately after placement, **(B** and **E**, respectively**)** region where healing chamber formation occurred between implant thread and cortical bone, and **(C** and **F**, respectively**)** trabecular bone region.*

general increase for all groups at 4 weeks (no significant differences among groups). Such result at 2 weeks showed that the microblasted RBM surface roughness and chemistry combination favored the early host–implant response, and that shortly after this observation period, no difference was evident because of the osseoconductive and biocompatible properties of other surfaces. The low degree of mechanical disruption between bone and implant observed in the histology slides after mechanical testing was likely caused by the proper specimen alignment and the slow controlled torque rate. Thus, mechanical disruption was observed only in a few histologic sections and did not compromise the histomorphologic and histomorphometric evaluations.[13,14,17]

In general, results from the histologic sections showed that all of the surfaces investigated were biocompatible and osseconductive, presenting bone in close contact with the implant surface at regions of cortical and trabecular bone. From a morphologic standpoint no differences were observed between all surfaces investigated. Woven bone was observed around all surfaces at 2 weeks, and initial replacement of woven bone by lamellar bone was observed for all surfaces at 4 weeks. No detrimental effect caused by blasting media particle presence on the surface was observed for the alumina-blasting and microblasted RBM groups at both implantation times.

Specific to different regions of the implant and its relationship with the surgical drilling dimensions, different healing patterns were observed throughout the implant length. At regions where intimate contact between cortical bone and implant surface existed immediately after placement, an appositional bone healing was observed.[16,27,29] Such healing pattern comprises interfacial remodeling with subsequent woven bone apposition in close contact with the implant surface,[16,27,29] as observed sequentially for all groups at 2 and 4 weeks. This type of configuration typically results in high degrees of implant primary stability.[27]

However, when the interplay between implant geometry and surgical drilling dimensions resulted in healing chamber formation, an intramembranous-like healing pattern was observed.[16,27,29] Healing chambers have been previously shown to be rapidly filled with woven bone throughout the volume occupied by the blood clot immediately after placement for osseointegration achievement.[16,17,27,29,30] In agreement with previous studies, the present results showed that in regions where healing chambers formed between implant and cortical bone, rapid woven bone filling occurred before or at 2 weeks, and initial remodeling comprising initial woven bone replacement by lamellar bone was observed by 4 weeks implatation time. The same morphologic evolution trend was observed at regions of trabecular bone.[31]

Although no significant differences were observed for both BIC and BAFO, a general increase was observed from 2 to 4 weeks in vivo, revealing that the time frames investigated in the present study were within the dynamic healing phases that occur at early implantation times. Within groups, the highest increase in BIC and BAFO values over time was observed for the biologic-blasting group, which at 4 weeks presented the highest mean values for BIC and BAFO among all surfaces evaluated. This observation was likely caused by the effect of higher amounts of calcium and phosphorus elements on the surface relative to the other groups, suggesting that their presence resulted in alteration in bone healing dynamics after implantation.[17-20,32]

CONCLUSIONS

The association of the implant macrogeometry and associated surgical technique with five different osseoconductive surfaces resulted in high degrees of osseointegration and biomechanical fixation. Although insight can be provided by evaluating five surfaces with distinct texture and chemistry, pinpointing

which of the surface parameters accounted for the differences in biomechanical and histomorphometric results is not possible, and experimental studies controlling these variables are warranted.

ACKNOWLEDGMENT

The authors report no conflicts of interest related to this study.

REFERENCES

1. Chuang SK, Tian L, Wei LJ, Dodson TB. Predicting dental implant survival by use of the marginal approach of the semi-parametric survival methods for clustered observations. *J Dent Res* 2002;81:851-855.
2. Chuang SK, Wei LJ, Douglass CW, Dodson TB. Risk factors for dental implant failure: A strategy for the analysis of clustered failure-time observations. *J Dent Res* 2002;81:572-577.
3. Albrektsson T, Gottlow J, Meirelles L, Ostman PO, Rocci A, Sennerby L. Survival of NobelDirect implants: An analysis of 550 consecutively placed implants at 18 different clinical centers. *Clin Implant Dent Relat Res* 2007;9:65-70.
4. Albrektsson T, Wennerberg A. Oral implant surfaces: Part 1 — Review focusing on topographic and chemical properties of different surfaces and in vivo responses to them. *Int J Prosthodont* 2004;17:536-543.
5. Albrektsson T, Wennerberg A. Oral implant surfaces: Part 2 — Review focusing on clinical knowledge of different surfaces. *Int J Prosthodont* 2004;17:544-564.
6. Coelho PG, Granjeiro JM, Romanos GE, et al. Basic research methods and current trends of dental implant surfaces. *J Biomed Mater Res B Appl Biomater* 2009;88:579-596.
7. Jimbo R, Ono D, Hirakawa Y, Odatsu T, Tanaka T, Sawase T. Accelerated photo-induced hydrophilicity promotes osseointegration: An animal study. *Clin Implant Dent Relat Res* 2009; in press.
8. Jimbo R, Sawase T, Baba K, Kurogi T, Shibata Y, Atsuta M. Enhanced initial cell responses to chemically modified anodized titanium. *Clin Implant Dent Relat Res* 2008;10:55-61.
9. Jimbo R, Sawase T, Shibata Y, et al. Enhanced osseointegration by the chemotactic activity of plasma fibronectin for cellular fibronectin positive cells. *Biomaterials* 2007;28:3469-3477.
10. Dohan Ehrenfest DM, Coelho PG, Kang BS, Sul YT, Albrektsson T. Classification of osseointegrated implant surfaces: Materials, chemistry and topography. *Trends Biotechnol* 2010;28:198-206.
11. Kang BS, Sul YT, Oh SJ, Lee HJ, Albrektsson T. XPS, AES and SEM analysis of recent dental implants. *Acta Biomater* 2009;5:2222-2229.
12. Moura CC, Souza MA, Dechichi P, Zanetta-Barbosa D, Teixeira CC, Coelho PG. The effect of a nanothickness coating on rough titanium substrate in the osteogenic properties of human bone cells. *J Biomed Mater Res A* 2010;94:103-111.
13. Coelho PG, Cardaropoli G, Suzuki M, Lemons JE. Early healing of nanothickness bioceramic coatings on dental implants. An experimental study in dogs. *J Biomed Mater Res B Appl Biomater* 2009;88:387-393.
14. Coelho PG, Lemons JE. Physico/chemical characterization and in vivo evaluation of nanothickness bioceramic depositions on alumina-blasted/acid-etched Ti-6Al-4V implant surfaces. *J Biomed Mater Res A* 2009;90:351-361.
15. Coelho PG, Marin C, Granato R, Suzuki M. Histomorphologic analysis of 30 plateau root form implants retrieved after 8 to 13 years in function. A human retrieval study. *J Biomed Mater Res B Appl Biomater* 2009;91:975-979.
16. Coelho PG, Suzuki M, Guimaraes MV, et al. Early bone healing around different implant bulk designs and surgical techniques: A study in dogs. *Clin Implant Dent Relat Res* 2010;12:202-208.
17. Granato R, Marin C, Suzuki M, Gil JN, Janal MN, Coelho PG. Biomechanical and histomorphometric evaluation of a thin ion beam bioceramic deposition on plateau root form implants: An experimental study in dogs. *J Biomed Mater Res B Appl Biomater* 2009;90:396-403.
18. Marin C, Granato R, Suzuki M, Gil JN, Piattelli A, Coelho PG. Removal torque and histomorphometric evaluation of bioceramic grit-blasted/acid-etched and dual acid-etched implant surfaces: An experimental study in dogs. *J Periodontol* 2008;79:1942-1949.
19. Mendes VC, Moineddin R, Davies JE. The effect of discrete calcium phosphate nanocrystals on bone-bonding to titanium surfaces. *Biomaterials* 2007;28:4748-4755.
20. Mendes VC, Moineddin R, Davies JE. Discrete calcium phosphate nanocrystalline deposition enhances osteoconduction on titanium-based implant surfaces. *J Biomed Mater Res A* 2009;90:577-585.
21. Buser D, Broggini N, Wieland M, et al. Enhanced bone apposition to a chemically modified SLA titanium surface. *J Dent Res* 2004;83:529-533.
22. Orsini G, Piattelli M, Scarano A, et al. Randomized, controlled histologic and histomorphometric evaluation of implants with nanometer-scale calcium phosphate added to the dual acid-etched surface in the human posterior maxilla. *J Periodontol* 2007;78:209-218.
23. Mendonça G, Mendonça DB, Aragão FJ, Cooper LF. Advancing dental implant surface technology — From micron- to nanotopography. *Biomaterials* 2008;29:3822-3835.
24. Leach R. Surface topography characterisation. In: *Fundamental Principles of Engineering Nanometrology*. William Andrew; 2009:211-258. [AQ6]
25. Stout K, Sullivan P, Dong W, et al. *Development of Methods for the Characterisation of Roughness in Three Dimensions*. Penton Press; 2000. [AQ7]
26. Donath K, Breuner G. A method for the study of undecalcified bones and teeth with attached soft tissues. The Säge-Schliff (sawing and grinding) technique. *J Oral Pathol* 1982;11:318-326.
27. Leonard G, Coelho P, Polyzois I, Stassen L, Claffey N. A study of the bone healing kinetics of plateau versus screw root design titanium dental implants. *Clin Oral Implants Res* 2009;20:232-239.
28. Wennerberg A, Albrektsson T. Suggested guidelines for the topographic evaluation of implant surfaces. *Int J Oral Maxillofac Implants* 2000;15:331-344.
29. Berglundh T, Abrahamsson I, Lang NP, Lindhe J. De novo alveolar bone formation adjacent to endosseous implants. *Clin Oral Implants Res* 2003;14:251-262.

30. Coelho PG, Granato R, Marin C, Bonfante EA, Janal MN, Suzuki M. Biomechanical and bone histomorphologic evaluation of four surfaces on plateau root form implants: An experimental study in dogs. *Oral Surg Oral Med Oral Pathol Oral Radiol Endod* 2010;109: e39-e45.
31. Quaranta A, Iezzi G, Scarano A, et al. A histomorphometric study of nanothickness and plasma-sprayed calcium-phosphorous-coated implant surfaces in rabbit bone. *J Periodontol* 2010;81:556-561.
32. Meirelles L, Melin L, Peltola T, et al. Effect of hydroxyapatite and titania nanostructures on early in vivo bone response. *Clin Implant Dent Relat Res* 2008;10:245-254.

Correspondence: Dr. Estevam A. Bonfante, Al. Octávio Pinheiro Brisola, 9-75, Bauru 17012-901, SP, Brazil. Fax: 55-14-32342566; e-mail: estevamab@gmail.com.

Submitted August 21, 2010; accepted for publication September 29, 2010.